cite as: Mitasova, H., Thaxton, C., Hofierka, J., McLaughlin, R., Moore, A., Mitas L., 2005, Path sampling method for modeling overland water flow, sediment transport and short term terrain evolution in Open Source GIS.
In: C.T. Miller, M.W. Farthing, V.G. Gray, G.F. Pinder eds., Proceedings of the XVth International Conference on Computational Methods in Water Resources (CMWR XV), June 13-17 2004, Chapel Hill, NC, USA, Elsevier, pp. 1479-1490.
https://www.sciencedirect.com/science/article/pii/S016756480480159X
https://doi.org/10.1016/S0167-5648(04)80159-X

Path sampling method for modeling overland water flow, sediment transport, and short term terrain evolution in Open Source GIS

Helena Mitasova[a], Chris Thaxton[b], Jaroslav Hofierka[c], Richard McLaughlin[d], Amber Moore[d], and Lubos Mitas[b]

[a]Department of Marine, Earth and Atmospheric Sciences North Carolina State University 1125 Jordan Hall, Raleigh, NC 27695, USA

[b]Department of Physics, North Carolina State University, Raleigh, NC 27695, USA

[c]Department of Geography and Geoecology, Presov University, Presov, Slovakia

[d]Department of Soil Science, North Carolina State University, Raleigh, NC 27695, USA

A path sampling method is proposed for solving the continuity equations describing mass flows over complex landscape surfaces. The modeled quantities are represented by an ensemble of sampling points which are evolved according to the corresponding Green function. The method enables incorporation of multi-scale/multi-process treatments. It has been used to develop simulation tools for overland shallow water flow and for sediment transport. The spatial pattern of sediment flow and net erosion/deposition is modeled using the closure relationship between sediment transport capacity and detachment developed for the USDA Water Erosion Prediction Project. The tools were recently implemented as modules in Open Source GRASS GIS. Their application is illustrated by the study of impact of land use and topography change on overland flow and sediment transport at North Carolina State University campus.

1. INTRODUCTION

The emergence of new mapping and automated monitoring technologies has created opportunities to improve the predictions of anthropogenic impacts on landscapes and to find sustainable solutions for development. Modeling of landscape processes plays an important role in this effort by allowing us to simulate the impact of proposed changes before they are implemented, and by providing tools to explore a wide range of alternatives. The new, high resolution data along with the new type of distributed models have a potential to bring the simulations to the level of realism and accuracy needed for decision making.

Traditional, spatially averaged models have limited capabilities to identify locations of problems (e.g., pollution sources) and the pattern of their propagation through landscapes. Also the possibilities to explore various alternatives of land use and optimal organization of landscape are restricted. Models based on continuous fields provide such insight, however, they are much more complicated in terms of their implementation and data requirements. Coupling with a Geographic Information System (GIS) makes applications of these models

more efficient, which makes them feasible for practical applications. In the early 90s, Geographic Resources Analysis and Support System (GRASS), as a public domain GIS, provided an environment for pioneering work in integrating GIS and landscape process modeling (e.g., [1–4]). While most of these models are now linked to proprietary GIS, the release of GRASS5.0 within the open source computational infrastructure [5] creates opportunities for development of new generation distributed models. Fully disclosed and available source code provides specialized libraries which make software implementation of the model simpler and more effective.

Current spatially distributed models, such as SIBERIA [6], CASC2d [7], CHILD [8], and SIMWE [9], have common theoretical foundations, however, the implementations were developed for different types of applications. In this paper, we focus on a modeling approach that supports spatial analysis of short term erosion/deposition patterns in landscapes with complex topography and land cover distribution, and provides information needed for better conservation and erosion prevention planning.

2. METHODS

To simulate the impact of a given configuration of topography, land cover, soil properties and rainfall event on spatial pattern of erosion/deposition and terrain evolution, we first solve the bivariate shallow water flow equation to obtain the spatial distribution of water flow depth. The water depth field is then used as an input to sediment transport model to estimate the distribution of net erosion/deposition and change in the elevation surface. The following sections describe the equations and numerical solution in more detail.

2.1. Shallow overland flow

For a shallow water flow, spatial variation in velocity with respect to depth can be neglected and the flow process can be approximated by the bivariate form of the St Venant equation [7]:

$$\frac{\partial h(\mathbf{r},t)}{\partial t} = i_e(\mathbf{r},t) - \nabla \cdot \mathbf{q}(\mathbf{r},t) \tag{1}$$

while the momentum conservation in the diffusion wave approximation has the form:

$$\mathbf{s_f}(\mathbf{r},t) = \mathbf{s}(\mathbf{r}) - \nabla h(\mathbf{r},t) \tag{2}$$

where $\mathbf{r} = (x, y)$ [m] is the position, t [s] is the time, $h(\mathbf{r}, t)$ [m] is the depth of overland flow, $i_e(\mathbf{r}, t)$ [m/s] is the rainfall excess = (rainfall − infiltration − vegetation intercept) [m/s], $\mathbf{q}(\mathbf{r}, t)$ [m^2/s] is the water flow per unit width, $\mathbf{s}(\mathbf{r}) = -\nabla z(\mathbf{r})$ is the negative elevation gradient, $z(\mathbf{r})$ [m] is the elevation, and $\mathbf{s_f}(\mathbf{r}, t)$ is the negative gradient of overland flow surface (friction slope). For a shallow water flow, with the hydraulic radius approximated by the normal flow depth $h(\mathbf{r}, t)$ [10] the unit discharge is given by:

$$\mathbf{q}(\mathbf{r},t) = \mathbf{v}(\mathbf{r},t)h(\mathbf{r},t), \tag{3}$$

where $\mathbf{v}(\mathbf{r}, t)$ [m/s] is the flow velocity. The system of equations (1) – (3) is closed using the Manning's relation between $h(\mathbf{r}, t)$ and $\mathbf{v}(\mathbf{r}, t)$:

$$\mathbf{v}(\mathbf{r},t) = \frac{C}{n(\mathbf{r})} h(\mathbf{r},t)^{2/3} |\mathbf{s_f}(\mathbf{r},t)|^{1/2} \mathbf{s_{f0}}(\mathbf{r},\mathbf{t}) \tag{4}$$

where $n(\mathbf{r})$ is the dimensionless Manning's coefficient, $C = 1\ [m^{1/3}/s]$ is the corresponding dimension constant [11], and $\mathbf{s_{f0}}(\mathbf{r}) = \mathbf{s_f}(\mathbf{r})/|\mathbf{s_f}(\mathbf{r})|$ is the unit vector in the friction slope direction. To account for spatially variable cover, necessary for land use management, we consider $n(\mathbf{r})$ and $i_e(\mathbf{r}, t)$ as explicitly location dependent.

To model erosion/deposition patterns and short term evolution of topography, we use the solution of continuity and momentum equations for a steady water flow that is close to kinematic wave approximation:

$$\partial h(\mathbf{r}, t)/\partial t = 0 \quad \longrightarrow \quad \nabla \cdot [h(\mathbf{r})\mathbf{v}(\mathbf{r})] = i_e(\mathbf{r}) \tag{5}$$

In order to incorporate the diffusive wave effects at least in an approximate way, we introduce a diffusion-like term $\propto \nabla^2[h^{5/3}(\mathbf{r})]$ into equation (5):

$$-\frac{\varepsilon(\mathbf{r})}{2}\nabla^2[h^{5/3}(\mathbf{r})] + \nabla \cdot [h(\mathbf{r})\mathbf{v}(\mathbf{r})] = i_e(\mathbf{r}) \tag{6}$$

where $\varepsilon(\mathbf{r})$ is a spatially variable diffusion coefficient.

The diffusion term, which depends on $h^{5/3}(\mathbf{r})$ instead of $h(\mathbf{r})$, makes the equation (6) linear in the function $h^{5/3}(\mathbf{r})$ which enables it to be solved using the path sampling method.

2.2. Sediment transport, soil erosion/deposition and terrain evolution

The general equation for change in topography due to erosion and deposition, adapted from [12] to three dimensions, is:

$$\frac{\partial z(\mathbf{r}, t)}{\partial t} = -\frac{1}{\varrho_b(\mathbf{r})}\nabla \cdot \mathbf{q}'_{\mathbf{s}}(\mathbf{r}, t) \tag{7}$$

where

$$\mathbf{q}'_{\mathbf{s}}(\mathbf{r}, t) = \mathbf{q}_{\mathbf{s}}(\mathbf{r}, t) - \gamma(\mathbf{r})|\mathbf{q}_{\mathbf{s}}(\mathbf{r}, t)|\nabla z \tag{8}$$

Here, $z(\mathbf{r}, t)$ [m] is the elevation at location $\mathbf{r}$ and time t, $\varrho_b(\mathbf{r})$ is bulk density $[kg/m^3]$ and γ is a diffusion coefficient. In it's basic form, equation (7) is simply the conservation equation for sediment mass commonly used in models that incorporate elevation change (e.g., [8,13–15]). A gravitational diffusion term captures the influence of local terrain slope on sediment transport [16]: the resulting *effective sediment load* (8) is either increased or decreased, delaying deposition (downslope) or encouraging it (upslope), respectively. The diffusion term is the primary mechanism for preventing the terrain from growing indefinitely and allowing the terrain to reach a state of dynamic equilibrium.

To estimate the sediment flow and net erosion/deposition we use the sediment continuity equation, which relates the change in sediment storage over time, and the change in sediment flow rate along the hillslope to effective sources and sinks [17,18]:

$$\frac{\partial[\rho_s c(\mathbf{r}, t)h(\mathbf{r}, t)]}{\partial t} + \nabla \cdot \mathbf{q}_{\mathbf{s}}(\mathbf{r}, t) = \text{sources} - \text{sinks} = D(\mathbf{r}, t) \tag{9}$$

where $\mathbf{q}_{\mathbf{s}}(\mathbf{r}, t)$ [kg/(ms)] is the sediment flow rate per unit width, $c(\mathbf{r}, t)$ [particle/m^3] is sediment concentration, ρ_s [kg/particle] is mass per sediment particle, $\rho_s c(\mathbf{r}, t)$ [kg/m^3] is

sediment mass density, and $D(\mathbf{r},t)$ [kg/(m^{2}s)] is the net erosion or deposition rate. The sediment flow rate $\mathbf{q_s}(\mathbf{r},t)$ is a function of water flow and sediment concentration:

$$\mathbf{q_s}(\mathbf{r},t) = \rho_s c(\mathbf{r},t)\mathbf{q}(\mathbf{r},t) \tag{10}$$

Again, we assume a steady state form of
the continuity equation:

$$\frac{\partial[\rho_s c(\mathbf{r},t)h(\mathbf{r},t)]}{\partial t} = 0 \quad \longrightarrow \quad \nabla \cdot \mathbf{q_s}(\mathbf{r}) = D(\mathbf{r}). \tag{11}$$

The sources and sinks term is derived from the assumption that the detachment and deposition rates are proportional to the difference between the sediment transport capacity and the actual sediment flow rate [19]:

$$D(\mathbf{r}) = \sigma(\mathbf{r})[T(\mathbf{r}) - |\mathbf{q_s}(\mathbf{r})|] \tag{12}$$

where $T(\mathbf{r})$ [kg/(ms)] is the sediment transport capacity, $\sigma(\mathbf{r})$ [m^{-1}] is the first order reaction term dependent on soil and cover properties. The expression for $\sigma(\mathbf{r}) = D_c(\mathbf{r})/T(\mathbf{r})$ is obtained from the following relationship [19]:

$$D(\mathbf{r})/D_c(\mathbf{r}) + |\mathbf{q_s}(\mathbf{r})|/T(\mathbf{r}) = 1 \tag{13}$$

The qualitative arguments, experimental observations, and values for $\sigma(\mathbf{r})$ are discussed, for example, by Foster and Meyer [19].

The sediment transport capacity $T(\mathbf{r})$ and detachment capacity $D_c(\mathbf{r})$ can be expressed by numerous simplified equations representing these rates under different conditions. In the WEPP model [20], they are expressed as functions of a shear stress:

$$T(\mathbf{r}) = K_t(\mathbf{r})[\tau(\mathbf{r})]^p \tag{14}$$

$$D_c(\mathbf{r}) = K_d(\mathbf{r})[\tau(\mathbf{r}) - \tau_{cr}(\mathbf{r})]^q \tag{15}$$

where $\tau(\mathbf{r}) = \rho_w\, g h(\mathbf{r}) \sin\beta(\mathbf{r})$ [Pa] is the shear stress, β [deg] is the slope angle, p and q are exponents, $K_t(\mathbf{r})$ [s] is the effective transport capacity coefficient, $K_d(\mathbf{r})$ [s/m] is the effective erodibility (detachment capacity coefficient), $\rho_w\, g$ is the hydrostatic pressure of water with the unit height, $g = 9.81$ [m/s^2] is the gravitational acceleration, $\rho_w = 10^3$ [kg/m^3] is the mass density of water, and $\tau_{cr}(\mathbf{r})$ [Pa] is the critical shear stress. The parameters and adjustment factors for the estimation of $D_c(\mathbf{r})$ and $T(\mathbf{r})$ are functions of soil and cover properties, and their values for a wide range of soils, cover, agricultural and erosion prevention practices were developed within the WEPP model [20].

Similarly as for the water flow equation, the steady state sediment flow equation (11) can be rewritten to include a small diffusion term $\propto \nabla^2\varrho(\mathbf{r})$:

$$-\frac{\omega}{2}\nabla^2\varrho(\mathbf{r}) + \nabla \cdot [\varrho(\mathbf{r})\mathbf{v}(\mathbf{r})] + \varrho(\mathbf{r})\sigma(\mathbf{r})|\mathbf{v}(\mathbf{r})| = \sigma(\mathbf{r})T(\mathbf{r}) \tag{16}$$

where ω [m^2/s] is the diffusion constant and $\varrho(\mathbf{r}) = \rho_s c(\mathbf{r})h(\mathbf{r})$ [kg/m^2] is the mass of water-carried sediment per unit area. On the left hand side of the equation (16), the first term

describes local diffusion, the second term is a drift driven by the water flow while the third term represents a velocity dependent 'potential' acting on $\varrho(\mathbf{r})$. The size of the diffusion constant is about one order of magnitude smaller than the reciprocal Manning's constant so that the impact of the diffusion term is relatively small. It represents local dispersion processes of the suspended flow, caused by microtopography which is not captured by the digital elevation model (DEM). The diffusion term can be modified to reflect impact of various processes.

2.3. Numerical solution by path sampling method

Most models of landscape processes are based on numerical solutions of governing partial differential equations by finite element [4], finite difference [3] or path sampling methods [9]. The path sampling method has several important advantages when compared with more traditional approaches. The method is very robust, can be easily extended into arbitrary dimension, is mesh-free and very efficient on parallel architectures.

Variety of path sampling methods have been explored in environmental applications such as simulation and transport of dissolved and suspended substances in water bodies [21,22], groundwater modeling [23] and soil erosion by overland flow [9]. The method has important applications in other areas such as quantum systems where the probability amplitude (wavefunction) can be mapped onto a "fluid" and used to solve the Schrodinger equation with special symmetry constraints. In that context, the methods are known as Green function Monte Carlo, diffusion Monte Carlo [24]. Equations (6) and (16) have a similar form in which a linear differential operator P acts on a nonnegative unknown function $f_0(\mathbf{r})$ (in our case, either $h(\mathbf{r})$ or $\varrho(\mathbf{r})$), while on the right hand side, there is a given source term $S(\mathbf{r})$ (either $i_e(\mathbf{r})$ or $\sigma(\mathbf{r})T(\mathbf{r})$):

$$Pf_0(\mathbf{r}) = S(\mathbf{r}) \tag{17}$$

Denoting by P^{-1} the inverse operator to P, the solution can be symbolically written as:

$$f_0(\mathbf{r}) = P^{-1}S(\mathbf{r}) \tag{18}$$

or explicitly, using the Green function:

$$f_0(\mathbf{r}) = \int_0^\infty \int G(\mathbf{r}, \mathbf{r}', t)S(\mathbf{r}')d\mathbf{r}'dt \tag{19}$$

$G(\mathbf{r}, \mathbf{r}', p)$ is given by the following time-dependent equation with an initial condition:

$$\frac{\partial G(\mathbf{r}, \mathbf{r}', t)}{\partial t} = -PG(\mathbf{r}, \mathbf{r}', t)\,; \;\; G(\mathbf{r}, \mathbf{r}', 0) = \delta(\mathbf{r} - \mathbf{r}'), \tag{20}$$

where $\mathbf{r}, \mathbf{r}'$ are positions, t is time and δ is the Dirac function. In addition, we assume that the spatial region is a delineated watershed with zero boundary condition which is fulfilled by $G(\mathbf{r}, \mathbf{r}', t)$. The corresponding equations can be interpreted as describing stochastic processes with diffusion and drift components (Fokker-Planck equations) and one can carry out the actual simulation of the underlying process using the path sampling method [25]. Our definition of the Green function effectively introduces time, the reason being that it enables us to consider both time dependent and stationary phenomena/processes on the

same footing. Let us therefore consider the following time-dependent partial differential equation:

$$\frac{\partial f(\mathbf{r},t)}{\partial t} = Pf(\mathbf{r},t) \tag{21}$$

where

$$Pf(\mathbf{r},t) = -\varepsilon\nabla^2 f(\mathbf{r}) + \nabla\cdot[f(\mathbf{r},t)\mathbf{v}(\mathbf{r})] - u(\mathbf{r})f(\mathbf{r},t) \tag{22}$$

so that the operator P includes diffusion (ε is a diffusion constant), drift, and potential (birth-decay) terms. The potential represents a rate term such as radioactive decay or proliferation in a chemical reaction. Starting from some initial $f(\mathbf{r},0)$ the solution of this equation can now be written as

$$f(\mathbf{r},t) = \exp(-tP)f(\mathbf{r},0) \tag{23}$$

This solves the given differential equation as can be verified by taking the derivative according to t.

For solving our transport equations (23), (6) and (16), we need the Green function (matrix element) $G(\mathbf{r},\mathbf{r}',t)$ for arbitrary $\mathbf{r},\mathbf{r}'$ so that we can write

$$f(\mathbf{r},t) = \int G(\mathbf{r},\mathbf{r}',t)f(\mathbf{r}',0)d\mathbf{r}' \tag{24}$$

Suppose that we know the Green function for some time slice τ. The solution at arbitrary multiple of τ can be found by iteration, e.g., the solutions at time τ and 2τ are given by

$$f(\mathbf{r},\tau) = \int G(\mathbf{r},\mathbf{r}',\tau)f(\mathbf{r}',0)d\mathbf{r}' \tag{25}$$

$$f(\mathbf{r},2\tau) = \int G(\mathbf{r},\mathbf{r}',\tau)f(\mathbf{r}',\tau)d\mathbf{r}' \tag{26}$$

etc.

If the time slice τ is small, using the Trotter-Suzuki formula one finds

$$G(\mathbf{r},\mathbf{r}',\tau) = C_N\exp[-|\mathbf{r}'-\mathbf{r}-\tau\mathbf{v}_0|^2/4\tau]\exp[-\tau(u(\mathbf{r}')+u(\mathbf{r}))/2] + O(\tau^3) \tag{27}$$

where C_N is the normalization constant of the Gaussian. Suppose now that we represent the function $f(\mathbf{r},0)$ as a density of sampling points (also called walkers)

$$f(\mathbf{r},0) \;\longrightarrow\; \sum_{m=1}^{M}\delta(\mathbf{r}-\mathbf{r}_m) \tag{28}$$

assuming that the density can be easily estimated by a histogram.

By decreasing the size of histogram bins and increasing the number of walkers one can get arbitrarily accurate approximation of a given function. If we rescale the function $f(\mathbf{r},0)$ by a constant, then the weight of the delta functions must change as well, so we introduce a walker weight w_m which gives the weight of each walker contribution to the bin. Therefore each walker is specified by its position and weight.

By substituting for $f(\mathbf{r},0)$ the set of walkers $\Sigma_m w_m \delta(\mathbf{r}-\mathbf{r}_m)$ to the equation above and by carrying out the integration we get for the walker with label m the following expression

$$\int G(\mathbf{r},\mathbf{r}',\tau) w_m \delta(\mathbf{r}'-\mathbf{r}_m) d\mathbf{r}' = C_N w_m \exp[-|\mathbf{r}_m-\mathbf{r}-\tau\mathbf{v}_0|^2/4\tau] \exp[-\tau(u(\mathbf{r})+u(\mathbf{r_m}))/2] \quad (29)$$

which is a Gaussian with renormalized weight. In order to carry out the next iteration in the same manner, we need to restore the delta-function/walker representation. This is done by *sampling* the Gaussian — finding a new position of the walker by drawing a random vector from a Gaussian distribution around $\mathbf{r}_m$, drifting by $\tau\mathbf{v}_0$ and updating the weight by the renormalization factor. Therefore the new position is given by

$$\mathbf{r}_m^{new} = \mathbf{r}_m + \tau\mathbf{v}_0 + \mathbf{g} \quad (30)$$

where $\mathbf{g}$ is a random vector with Gaussian components with variance τ while the updated weight reads

$$w_m^{new} = w_m \exp[-\tau(u(\mathbf{r}_m^{new}) + u(\mathbf{r}_m))/2] \quad (31)$$

The walker representation is based on duality between the particle and field representation of spatially distributed phenomena. Within this concept, density of particles in space defines a field and vice versa, i.e., field is represented by particles/samples with corresponding spatial distribution. Using this duality, processes can be modeled as evolution of fields or evolution of spatially distributed particles as described above.

The solution is then described as a function with statistical error proportional to $1/\sqrt{M}$ where M is the number of walkers. The solution for steady state can be obtained in two ways. One possibility is to evolve the time-dependent solution until the steady state is reached. Statistically, this is less efficient since the equilibration part of walker paths are thrown away. The second option is to start from the initial walker distribution proportional to the source $S(\mathbf{r})$ which is then evolved as given above. The steady-state solution is obtained by accumulation of the evolving source over the relevant period (i.e., until all the walkers flow out or die out), effectively performing the corresponding integral over time.

The accumulation process can be also interpreted as an approximation of a dynamical solution for shallow water flow, in which velocity is mostly controlled by terrain slope and surface roughness rather than by water depth and friction slope, and therefore its change over time at a given location is negligible. The robustness of the path sampling method enables the use of a very wide range of input data and complex conditions that can be modeled without manually editing the input data, as it is common with traditional methods. It can be therefore used efficiently for exploration of large number of landscape configurations, needed for various applications, including conservation planning and sediment control.

multiscale formulation using nested grids

Both *spatially variable accuracy* and *resolution* can be implemented by reformulating the solution through the Green function given by equation (18). The integral equation (18) can be multiplied by a *reweighting* function $W(\mathbf{r})$:

$$W(\mathbf{r}) f_0(\mathbf{r}) = \int_0^\infty \int W(\mathbf{r}) G(\mathbf{r},\mathbf{r}',t) S(\mathbf{r}') d\mathbf{r}' dt = \int_0^\infty \int G^*(\mathbf{r},\mathbf{r}',t) S(\mathbf{r}') d\mathbf{r}' dt \quad (32)$$

which is equal to the appropriate increase in accuracy ($W(\mathbf{r}) > 1$) in the regions of interest while it is unity elsewhere. The function $W(\mathbf{r})$ can change (abruptly or smoothly) between regions with unequal resolutions and in fact, can be optimally adapted to the quality of input data (terrain, soils, etc) so that the accurate solution is calculated only in the regions with correspondingly accurate inputs. The reweighted Green function $G^*(\mathbf{r}, \mathbf{r}', t)$, in effect, introduces higher density of sampling points in the region with large $W(\mathbf{r})$. The statistical noise will be spatially variable as $\approx 1/[W(\mathbf{r})\sqrt{M}]$, where M is the average number of samples resulting in the accuracy increase for the areas with $W(\mathbf{r}) > 1$. The multiscale approach was presented for modeling with spatially variable accuracy and homogeneous resolution in [26] and for spatially variable resolution in [27].

3. GIS IMPLEMENTATION AND APPLICATION

To increase the efficiency in data preparation and results analysis the method was integrated within GRASS GIS. Its functionality is being tested in several locations in the North Carolina Triangle area, with ongoing monitoring that will support the specific model calibration and validation for various conditions.

3.1. Implementation in GIS

The path sampling approach can be used to simulate a wide range of fluxes described by continuity equations. The algorithm that propagates the walkers was therefore implemented as a library that can be used to build models for other types of transport. This library was then used to build two specific modules for simulation of water flow and for sediment transport and erosion/deposition. Both modules are fully integrated with GRASS GIS and are executed from within the system. A wide range of GRASS GIS tools is used to preprocess the georeferenced input data as well as to analyze and visualize the outputs.

The module **r.sim.water** solves the equation (6) and computes maps representing spatial distribution of steady state water depth and discharge. Optionally, it is possible to output time series of raster maps representing evolution of water flow until it reaches steady state. Input data include raster maps representing elevation, first-order partial derivatives of elevation surface, rainfall excess, and Manning's surface roughness coefficient. Elevation surface gradient can be combined with gradients representing channels or other features that control water flow. There are a number of parameters that allow the user to control the simulation by adjusting the number of walkers, number of iterations and diffusion, including a modified diffusion term which enables to overcome elevation depressions or obstacles when accumulated water depth exceeds a threshold water depth value. Number of iterations effectively controls the duration of simulated event. It is also possible to output series of site maps representing spatial distribution of walkers at different simulation times.

The module **r.sim.erosion** solves the equation (16) and computes maps representing spatial distribution of steady state sediment flow rate, sediment concentrations and net soil erosion/deposition rate. Input data include raster maps representing elevation, first-order partial derivatives of elevation surface, water depth (computed e.g., by **r.sim.water**), detachment capacity coefficient, transport capacity coefficient, critical shear stress and Manning's surface roughness coefficient. Optionally, it is possible to output transport

capacity map and transport capacity-limited erosion/deposition rates. Time series of raster maps representing evolution of sediment flow and erosion/deposition for the given water depth can also be produced. Similarly as for water, the simulation can be controlled by adjusting the number of walkers, number of iterations and a diffusion term.

The module **r.terradyn** is a terrain evolution routine for small watersheds. Currently, it is implemented as a shell script run within GRASS GIS that solves equation (7), producing a time series of updated elevations based on the distributed erosion/deposition rates from **r.sim.sediment**. At each iteration, the terrain change is smoothed via the GRASS GIS module **r.neighbors**. Even with the additional diffusion term in (8), this step is critical for the suppression of numerical noise over a large number of iterations. Partial derivatives of the elevation surfaces are computed using the module **r.slope.aspect**. The user can define the same control variables and spatially distributed input raster files as with **r.sim.water** and **r.sim.sediment**, as well as the number of terrain update iterations and the smoothing parameter. Currently, the bulk density ϱ_b and the gravitational diffusion coefficient γ are user-definable scalars; however, since these parameters should be a function of soil type, we plan to implement them as distributed variables in the future. In addition, the user can opt to dynamically redefine the transport and detachment coefficients and the critical shear stress based on the water depth and/or depositional history.

3.2. Application in North Carolina

The model is currently being tested at several locations in North Carolina with ongoing changes in land use and monitoring of water flow and sediment transport. The first test area is at the Southwest section of the North Carolina State University Centennial Campus that is being transformed from forest and meadows to developed area with educational and recreational facilities (Figure 1). To reduce the negative effects of construction on soil erosion and water pollution, sediment control measures need to be installed. The presented example explores the use of GIS and simulations to better assess the need for sediment control measures and plan their most effective locations. During the school construction, 3 large checkdams were installed to control sediment. In near future, the construction of golf course will lead to removal of a large portion of the current forest. To simulate the impact of this development with conservation measures, several landscape models were created, representing the current and planned elevation surfaces and various configurations of landcover including: (a) current state, (b) start of construction without control measures, (c) construction with extended buffers, (d) staged construction, (f) finished grading before planting, and (g) finished golf course. Water and sediment flow as well as erosion/deposition were then simulated for each configuration for a 42mm/hr, steady rainfall for a duration of 1 hour. The results are illustrated by Figure 1 and Table 1. As expected, the simulations demonstrate that the construction will lead to substantial increase in runoff and sediment transport. Surprisingly, the major negative impact is predicted outside the actual disturbed area, in the form of erosion due to concentrated flow within the preserved mandatory buffers. The channels need to be surveyed prior and during the construction to verify this result. Relative efficiency of different conservation measures was quantified by comparing the total runoff, sediment yield, and total erosion for two types of extended buffers and staged construction.

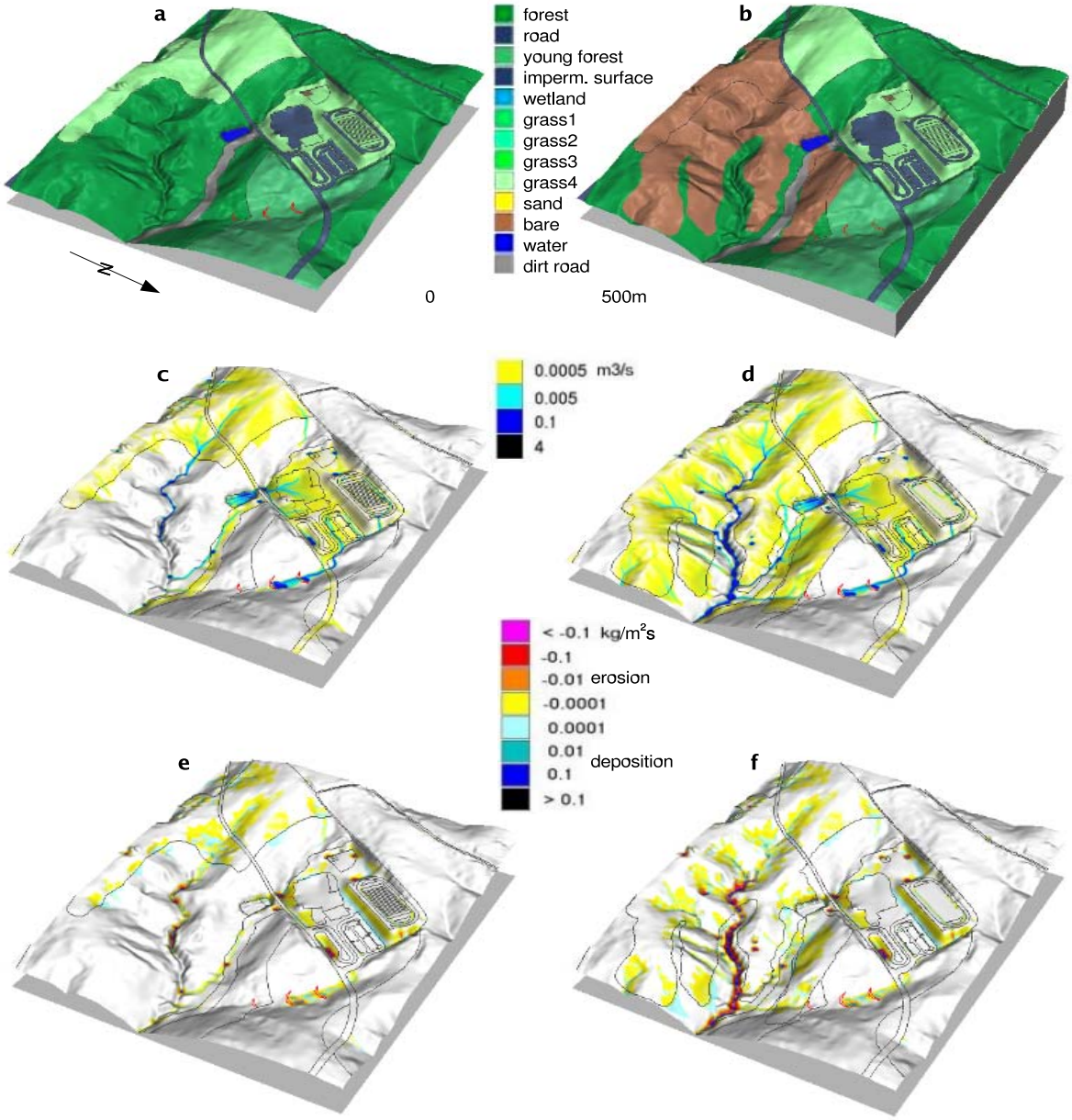

Figure 1. Spatial pattern of land cover (a,b), overland flow (c,d) and net erosion/deposition (e,f) before and at the start of construction. The largest increase in erosion is predicted within the protective buffer due to increased water flow. Simulations also show the effectiveness of large checkdams in controlling water flow from the parking lot.

The simulations show that the standard buffers provide very limited protection (Figure 1); however, their extension into most of the areas with concentrated flow, using the cover that preserves high infiltration and vegetation intercept, substantially reduces the negative impact. The effectiveness of staged construction varied depending on the size and location of the disturbed area; it was not very effective when entire the "half-watershed" that included several concentrated flow areas was disturbed at once (Figure 1, stage cs1).

Table 1
Discharge and sediment yield at the outlet of the subwatershed with the planned golf course, and total erosion rate for the entire study area (100acres) at different stages of development and conservation measures. Discharge and sediment yield equal to zero reflect the impact of numerous depressions in the modeled subwatershed for stages that produce lower runoff.

land use	discharge [m^3/s]	sediment yield [kg/s]	erosion rate [kg/s]
pre-development	0.0	0.0	84.
current	0.0	0.0	87.
start of construction	0.46	0.26	968.
extended buffers grass	0.45	0.25	337.
extended buffers forest	0.0	0.0	142.
staged constr. section 1	0.30	0.18	771.
staged constr. section 2	0.16	0.11	216.

4. CONCLUSIONS

High resolution, spatially distributed simulations provide new insight into the spatial aspects of impacts of disturbances in complex landscapes. Integration with GIS supports efficient design and evaluation of various configurations of conservation measures providing valuable information for erosion prevention and sediment control. The path sampling method provides the robustness necessary for simulating diverse landscapes and complex interactions. Future development, based on the combination of finite difference and path sampling method, is focusing on expanding the capabilities for more realistic modeling of dynamics of water and sediment flow and terrain evolution. Routine applications will require comprehensive model calibration and validation that will be based on the established and new monitoring and experiments at sites in North Carolina.

REFERENCES

1. C.C. Rewerts and B.A. Engel, ASAE Paper No.91-2621 (1991).
2. R. Srinivasan and J.G. Arnold, Water Resources Bulletin 30 (1994) 453.
3. B. Saghafian, in: GIS and Environmental Modeling: Progress and Research Issues, M.F. Goodchild, L.T. Steyaert and B.O. Parks (eds.), GIS World Inc. (1996) 205.

4. B.E. Vieux, N.S. Farajalla and N. Gaur, in: GIS and Environmental Modeling: Progress and Research Issues, M.F. Goodchild, L.T. Steyaert and B.O. Parks (eds.), GIS World Inc. (1996) 199.
5. M. Neteler and H. Mitasova, Open Source GIS: A GRASS GIS Approach, Kluwer Academic Press, Boston, 2002.
6. G.R. Willgoose, and Y. Gyasi-Agyei, in: Proceedings of the APCOM XXV Conference, Brisbane (1995) 555.
7. P.Y. Julien, B. Saghafian, and F.L. Ogden, Water Resources Bulletin 31 (1995) 523.
8. G. Tucker, S. Lancaster, N. Gasparini and R. Bras, in: Landscape Erosion and Evolution Modeling, R.S. Harmon and W.W. Doe (eds.), Kluwer, New York (2001) 349.
9. L. Mitas and H. Mitasova, Water Resources Research 34 (1998) 505.
10. I.D. Moore and G.R. Foster, in: Process Studies in Hillslope Hydrology, M.G. Anderson and T.P. Burt (eds.), John Wiley (1990) 215.
11. S.L. Dingman, Fluvial hydrology, Freeman, New York, 1984.
12. T.V. Karrambas and C. Koutitas, J. of Waterway, Port, Coastal and Ocean Engineering 128 (2002) 102.
13. G. Parker, C. Paola and S. Leclair, J. of Hydraulic Engineering, 126 (2000) 818.
14. C. Paola and R. Seal, Water Resources Research, 31 (1995) 1395.
15. W.E. Dietrich, C.J. Wilson, D.R. Montgomery, J. McKean, J. of Geology, 101 (1993) 259.
16. K. Horikawa, Nearshore dynamics and coastal processes, University Tokyo Press, Tokyo, 1988.
17. C.T. Haan, B.J. Barfield and J.C. Hayes, Design Hydrology and Sedimentology for Small Catchments, Academic Press (1994) 242.
18. R.S. Govindaraju and M. L. Kavvas, J. of Hydrology 127 (1991) 279.
19. G.R. Foster and L.D. Meyer, in: Sedimentation: Symposium to Honor Prof. H.A. Einstein, H. W. Shen (ed.), Colorado State University, Ft. Collins, CO (1972), 12.1.
20. D.C. Flanagan and M.A. Nearing (eds.), USDA-Water Erosion Prediction Project, NSERL report no. 10, National Soil Erosion Lab., USDA ARS, Laffayette, IN, 1995.
21. Danish Hydrologic Institute, MIKE21 PA, http://www.dhisoftware.com/ (2003).
22. K.N. Dimou and E.E. Adams, Estuarine, Coastal and Shelf Science 33 (1993) 99.
23. A.F.B. Thompson and L.W. Gelhar, Water Resources Research 26 (1990) 2541.
24. M.W.C. Foulkes, L. Mitas, R.J. Needs and G. Rajagopal, Rev. Mod. Phys. 73 (2001) 33.
25. C.W. Gardiner, Handbook of Stochastic Methods for Physics, Chemistry, and the Natural Sciences, Springer, Berlin, 1985.
26. L. Mitas and H. Mitasova, in: Modelling Soil Erosion, Sediment Transport and Closely Related Hydrological Processes, W.Summer, E. Klaghofer and W.Zhang (eds.), IAHS Publication no. 249 (1998) 81.
27. H. Mitasova and L. Mitas, in: Landscape erosion and landscape evolution modeling, Harmon R. and Doe W. (eds.), Kluwer, New York (2001) 321.